

Variability in the Inverse-Compton X-ray Flux from the Jet in Quasar 3C 345

S. C. Unwin

Department of Physics, Mathematics and Astronomy,
Caltech 220-47, Pasadena, CA 91125

A. E. Wehrle

Infrared Processing and Analysis Center, Jet Propulsion Laboratory,
Caltech 100-22, Pasadena CA 91125

A. P. Lobanov and J. A. Zensus

National Radio Astronomy Observatory, 520 Edgemont Road, Charlottesville, VA 22903

G. M. Madejski

Code 666, Goddard Space Flight Center, Greenbelt, MD 20771

and

M. J. Aller and H. D. Aller

Astronomy Department, University of Michigan, Ann Arbor, MI 48109-1090

ABSTRACT

We present the results of the first systematic study of *correlated variability* in the X-ray emission and the parsec-scale radio structure of the 'superluminal' quasar 3C 345. This quasar is one of a class of core-dominated flat-spectrum radio sources which are believed to emit X-rays via the synchrotrons self-Compton process. By studying its variability in X-rays, we can test this hypothesis for 3C 345 by modeling the expected inverse-Compton flux from the parsec-scale jet, using parameters derived from multifrequency VLBI imaging. Since the predicted X-ray flux is very sensitive to the physical parameters of the compact radio-emitting regions, a study of variability, with quasi-simultaneous X-ray and VLBI data, is of particular interest because it is less sensitive to assumptions in the adopted model.

The soft X-ray flux density of 3C 345 was observed by the ROSAT PSPC instrument at five epochs during 1990 - 93, during which time its flux density varied by a factor of two, but with no change in spectral index. The X-ray points closely track the high-frequency radio flux light curve. Using a series of VLBI images, we followed the time evolution of spectral shapes and angular sizes of the nucleus and the strongest jet component 'C7', at a distance of $\simeq 0.5$ mas (2 pc) from the nucleus, and derived physical parameters for the components. We find that component C7, not the nucleus, is the dominant generator of the observed X-rays during 1992-93. For the nucleus, we applied

the inhomogeneous-jet model of König, and found find that it under-predicts the X-ray flux for any plausible combination of physical parameters derived from observation. A homogeneous sphere, with flux density peaking at a few GHz, is adequate for modeling the evolution of C7. This sphere model requires that C7 dominated the X-ray emission, unless its Doppler factor is $\gg 10$. This contrasts with the situation at epoch 1990.55, for which comparable data (Unwin et al. 1994) showed that the nucleus and C5 (the dominant jet feature at that time) both contributed to the X-ray emission. We discuss the lack of detectable γ -rays from 3C 345 in relation to other γ -ray loud blazars with which it shares many observational properties. Combining the superluminal speed (from VLBI) and Doppler factor deduced from the synchrotrons self-Compton calculation, we solve for the jet kinematics at the position of C7, and find that the jet bends away from the line of sight (from $\theta \simeq 2^\circ$ to $\simeq 10^\circ$), and accelerates from $\gamma \simeq 5$ to $\gtrsim 10$ over the range of (deprojected) distance from the nucleus of $\simeq 3$ to $\simeq 20$ pc.

Subject *headings*: quasars: individual: (3C 345) — galaxies: jets — radiation mechanisms: non-thermal — radio continuum: galaxies — X-rays: galaxies

1. Introduction

The quasar 3C 345 ($z = 0.595$; Moore & Stockman 1984, Hewitt & Burbidge 1993) is perhaps the best-studied of all ‘superluminal’ radio sources (apparent internal proper motion $\beta_{\text{obs}}c$ in excess of c). Its radio structure is dominated by a flat-spectrum core, with a one-sided kiloparsec-scale jet and a faint halo (Kollgaard, Wardle, & Roberts 1989). Superluminal motion is detected in several components in the parsec-scale core with VLBI; their evolution has been monitored with imaging at cm-wavelengths since the late 1970s (Unwin & Wehrle 1992, Zensus, Cohen, & Unwin 1995, Zensus et al, 1996). These images, typically made at intervals of a few months, span the cm-wavelength band from 1.7 GHz through 43 GHz. Lobanov (1996) has compiled a database of parameters extracted from a total of 60 VLBI images which can be used in several ways to test models of the kinematics and evolution of the parsec-scale jet. Qian et al. (1996) and Steffen et al. (1995) have tested the hypothesis that the curved trajectories of superluminal components result from following paths which lie on the surface of a broad cone. Lobanov & Zensus (1996) show that the evolution of the spectral shape of an earlier jet component ‘C5’, which dominated the jet in the late 1980s, is consistent with the evolution expected of emission behind a propagating plane-parallel shock in the jet, Roberts et al. (1994) have studied the jet evolution through linear polarization VLBI at 5 GHz, and find that most of the polarized flux originates in the moving components, not the core - a result which may be common in quasars (Cawthorne et al. 1993). Leppanen, Zensus & Diamond (1995) showed that the magnetic field near the base of the jet is predominantly transverse to the jet, consistent with compression by shocks in the underlying flow.

3C 345 is bright and variable in most wavebands, making it an excellent candidate for broad-

band variability studies. Hagen-Thorn et al. (1996) performed multi band photometry in the optical and near-IR in 1991-92; they showed that the variable component has a mean spectral index in those bands of $\alpha_{\text{IR}} = 1.06$ which steepened to $\alpha_{\text{opt}} = 1.66$ in the optical. Since this continuum is probably an extension of the power-law from the millimeter and far-IR bands (Gear et al. 1994; Impey & Neugebauer 1988), we can use the slope as a constraint on emission models (see Section 4). It is also a non-thermal X-ray source (Cohen et al. 1983; Unwin et al. 1994); the X-rays are believed to originate in the jet via inverse-Compton scattering of low-energy photons. Except for 3C 279 and 3C 273, little is known about the X-ray variability of optically violently variable (OVV) blazars (McHardy 1996). This paper presents the most complete data so far on 3C 345. Previous studies (Unwin et al. 1994; Zensus, Cohen, & Unwin 1995) have shown that superluminal motion and synchrotron self-Compton (SSC) X-ray emission independently require the jet to be relativistic, from which a self-consistent picture of the jet kinematics can be built. In fact, bulk relativistic motion (Doppler factor $\delta > 1$) is required in most blazars (e.g. Readhead 1994; Gujosa & Daly 1996). The only band in which 3C 345 remains undetected is in γ -rays (an upper limit from the EGRET experiment on CGRO is given by Fichtel et al. 1994). We discuss possible reasons for this non-detection in Section 5.

Multiwavelength campaigns have been undertaken by several groups to provide important constraints on models of the blazar emission process (Bregman et al. 1986, Webb et al. 1994). A complete understanding is still some distance away, but greatly improved recent data (especially on broadband variability, and VLBI imaging; Stevens et al. 1996, Unwin et al. 1994) should discriminate between the main classes of proposed models (see review by Marscher 1996, and Section 5).

In this paper we study the time evolution of the core of 3C 345 and the brightest jet components C6 and C7, during 1991 - 93. We test the inverse-Compton model for the X-ray emission by comparing model predictions with quasi-simultaneous observations in X-rays with the ROSAT Position Sensitive Proportional Counter (PSPC). We have a total of five X-ray epochs for which reasonably complete radio spectra and angular sizes can be derived from the VLBI database. By examining time-variability in the relation between X-ray and radio properties, we can eliminate many systematic errors resulting from over-simplified modeling - we are more interested in *changes* in derived parameters than their absolute values,

Some of the questions we can answer with variability data are the following: What is the amplitude and timescale of variability in X-rays from 3C 345? Is there any variation in spectral index? Are X-ray flux density variations correlated with radio properties, such as total flux density at different frequencies? Are X-ray variations associated with individual components in the relativistic jet, and do they correlate with angular size or spectral shape? Can variability provide any new information on the geometry and dynamics of the parsec-scale jet?

X-ray observations of 3C 345 and methods of data reduction are presented in Section 2, and the estimation of VLBI parameters from the VLBI database are described in Section 3. Section 4 describes the models we have used to predict the X-ray emission from the nucleus, and Section

5 discusses some implications of our results for models of the broad-band emission, and addresses the hard γ -ray non-detection of 3C 345. We summarize our conclusions in Section 6. In this paper we use a Hubble constant $H_0 = 100 h \text{ km s}^{-1} \text{ Mpc}^{-1}$ and $q_0 = 0.5$; for $z = 0.595$ the angular scale is $3.79 h^{-1} \text{ pc/mas}$; where necessary, we set $h = 1$. Spectral index α is defined by $S_\nu \propto \nu^{-\alpha}$; the X-ray photon index is $\Gamma = 1 + \alpha$. We adopt the nomenclature of Lobanov & Zensus (1996), and references therein, for identifying discrete components in the jet.

2. X-ray Monitoring Results

3C 345 was observed by the ROSAT PSPC instrument, sensitive in the 0.1 – 2.4 keV range, 6 times during 1990- 1993. The details of the observations are given in Table 1, Three of the observations were pointed at other targets close to 3C 345, such that the image of 3C 345 was off-axis, partially under the PSPC ribs. However, since all the observations were obtained while the ROSAT spacecraft was operated in the “wobble” mode (designed to eliminate the effect of the PSPC support structure on the source data), it was possible to correct for both the vignetting and for partial obscuration by the ribs (see Appendix A). In all cases, the source images were consistent with a point source, For all observations, the source data were extracted from a circular region around the optical position of the source. For the on-axis observations, we used a region 2 arc min in radius, while for the off-axis observations, we used a region 3 arc. min in radius. The background was extracted from source-free regions at least several times larger than the source regions. No evidence was found for variability within an observation (i.e. between spacecraft orbits). In July 1992 as well as in March 1993, pairs of observations were separated by a few days in time (Table 1), and no variability ($< 10 \%$) is observed on that timescale. In subsequent analysis, we used mean values for the July 1992 and March 1993 observations.

Observations typically comprised several continuous records of $\sim 1 - 2$ ks in length, too short to obtain a good measurement of the X-ray spectrum. We thus fitted all the data records from an observation (selecting PSPC channels 12 to 211, i.e., an energy range of 0.12 - 2.1 keV) simultaneously, using the appropriate PSPC response matrices (for the 1990.55 observation PSPC “C” was used, while for the remaining ones it was PSPC “B”). For the spectral fits we used the package XSPEC (Shafer et al, 1990), adopting a simple, absorbed power-law model (photon index $\Gamma = 1 + \alpha$). None of the spectral fits showed evidence of spectral lines, or departures from a simple power-law. The absorption is by a column density N_{H} of a neutral gas, with abundances and cross-sections as given in Morrison & McCammon (1983).

We first treated as free parameters the flux density at each epoch, along with a single column density and photon index. This yielded $\chi^2 = 295$ (with 230 degrees of freedom). The corresponding spectral parameters were $\alpha = 0.97 \pm 0.09$, $N_{\text{H}} = 1.2 \pm 0.2 \times 10^{20} \text{ cm}^{-2}$ (all errors are 90% confidence regions for a single parameter of interest, i.e. corresponding to $\chi^2_{\text{min}} + 2.7$). Formally, the reduced χ^2 from the fit is unacceptably large, but the ROSAT observations could well be affected by systematic: they were performed using two different detectors, and some pointings were off-axis,

where the PSPC calibration may be less than optimal; further analysis of this discrepancy must await recalibration of the PSPC. The derived value of absorption is somewhat larger than the Galactic value of $N_{\text{H}} = 0.74 \times 10^{20} \text{ cm}^{-2}$ quoted by Elvis, Lockman, & Wilkes (1989), measured using 21 cm techniques. However, we note that 3C 345 resides in a region of extremely low column density, and thus the fractional systematic errors in the HI measurement may be larger than for other sources.

The fit degrades only slightly ($\chi^2 = 316$ with 229 degrees of freedom) when the column density is fixed at the Galactic value, so we adopted this value and re-fitted the data, which yielded $\alpha = 0.74 \pm 0.04$. Derived source flux densities changed by $< 10\%$ when N_{H} is fixed. There is no evidence for variability of the spectral parameters from one observation to another. The unabsorbed 1 keV flux densities quoted in Table 1 use $\alpha = 0.74$, and $N_{\text{H}} = 0.74 \times 10^{20} \text{ cm}^{-2}$ for the count rate - to - flux density conversion,

The X-ray emission is spatially unresolved by the PSPC (resolution ≈ 25 arcsec FWHM). Since the variable part of the emission changes on timescales of a year or less, it must originate on scales smaller than the 15-kpc radio jet (Kollgaard, Wardle, & Roberts 1989) or the the diffuse (~ 20 -arcsec) halo (Murphy, Browne, & Perley 1993). Based on SSC models (Section 4), the emission region lies within ~ 50 pc of the nucleus.

Figure 1 shows the X-ray and high-frequency radio flux density measurements. The two pairs of close X-ray measurements in Table 1 show that the variability timescale is longer than several days. The apparent strong correlation between X-ray and high-frequency radio flux density suggests that the characteristic timescale for large changes is of order weeks to months. However, as indicated below, we are not required to make that assumption in our analysis of the expected inverse-Compton emission, because we can reliably interpolate the radio imaging data to the X-ray epochs. From the shapes of the flux density curves, it is clear that the X-rays follow the highest frequencies (≥ 90 GHz) most closely; a detailed analysis of the (radio through millimeter-wave) flare is given by Stevens et al. (1996), and is discussed further in Section 5.

Since there is no evidence for variability in the X-ray spectral index before or after a rise of more than a factor of two in flux density (1990 - 1993), it is unlikely that the X-ray emission arises from two components, say, a hard and a soft component, each with different time histories. For the same reason, we can rule out any significant thermal emission from kiloparsec scales.

3. VLBI Monitoring Results

Results from a long program of monitoring the parsec scale structure with VLBI are published elsewhere (Unwin & Wehrle 1992, Zensus et al, 1996). All the VLBI images show a relativistic jet, which appears one-sided due to Doppler-boosting. Components in the jet are well-separated at 22 GHz, but are often blended at lower frequencies. Unfortunately, there is sparse imaging data at 43 GHz (the image by Krichbaum et al. 1993 is of too low dynamic range to include in the

present analysis, but shows that the nucleus dominates at high frequencies). Careful comparison of adjacent epochs at the same frequency and adjacent frequencies, coupled with model-fitting of a small number of homogeneous spherical components to the (u, v) data, enables physical parameters to be reliably extracted in most cases (see Lobanov 1996 for a detailed discussion). Figure 2 shows a representative image at 22 GHz from Lobanov; most of the identifiable parsec-scale components (or ‘knots’) persist several years, and yield measurable proper motions. Zensus, Cohen, & Unwin (1995) have parameterized the kinematics of the apparent component motions projected onto the plane of the sky; they find acceleration and curvature which are indicative of either jet precession or hydrodynamic instabilities.

Comparison of multifrequency VLBI data shows the well-known trend in spectral index: flat or rising ($\alpha < 0$) spectrum in the core, and ‘normal’ ($\alpha \simeq 0.7$) spectra in the jet components. In cases where the components are well-separated even at low frequencies (1.7 and 5 GHz), where the resolution is correspondingly lower, a peak in the spectrum can often be measured. This spectral ‘turnover’ point (ν_m, S_m) is one of the critical parameters for both homogeneous and inhomogeneous models of the broad-band continuum emission (Section 4).

Since the X-ray data sampling is sparse (9 -12 months), relative to the VLBI coverage (3 -6 months), and centimeter-wavelength radio total-flux monitoring (every few days at UMRAO [Aller, Aller, & Hughes 1992] and roughly monthly above 90 GHz [Stevens et al. 1996]), we interpolated the radio parameters to the X-ray epochs. This interpolation is easily done at low frequencies, even though the VLBI epochs are widely spaced. At 22 GHz, the VLBI data are better sampled, but the single-dish flux indicates that variability is more rapid. This does not cause significant errors in parameter estimation, provided the correspondence between features at successive epochs and frequencies is made correctly,

To estimate physical parameters for the main features in each image, we fitted a source model comprising a small number of homogeneous spheres to the calibrated (u, v) data in the VLBI database. The number of model components was dictated by the need to represent the main features in the images. In this way the complexity of a 2-D image is reduced to a small number of model parameters. Details of the model fitting procedure are given by Lobanov (1996). More than 60 VLBI images went into the spectral analysis we discuss here. The 1990 data, along with a model analysis and a discussion of the limitations of the model, are given in Unwin et al. (1994). In this analysis, we consider only the two dominant components from those epochs: the core itself (‘I’), and jet component ‘C7’. Component C6 and components emitted earlier from the core (C5, et c.) are much weaker and more extended; as we show below, they are therefore not of interest in constraining models of the broad-band emission. Note that C5 was the dominant jet component in 1990 (Unwin et al. 1994).

Figure 3 shows the radio spectra of the principal components in the parsec-scale jet, evaluated at epoch 1992.67, along with the total source flux density from the 3C 345 VLBI database (Lobanov 1996), the UMRAO database, and Stevens et al, (1996). Also shown are fits of simple models which are used to extract the component ‘turnover’ parameters, as discussed in the next Section.

4. Testing models of **the X-ray emission**

4.1. X-ray variability

The five X-ray flux density measurements are directly correlated with the total flux density at 14.5 GHz and higher frequencies (Fig. 1), both in amplitude range and variability timescale. Since the radio variability is known to arise in the nucleus and parsec-scale jet components imaged directly with VLBI, this is strong evidence that the X-ray emission originates in the parsec-scale jet.

In models in which the synchrotrons self-Compton (SSC) process plays an important role in X-ray production (Königl 1981, Bloom & Marscher 1996, and references therein) a correlation is expected because the process which generates the radio outburst increases both the electron energy and the number density of synchrotrons photons available for up-scattering to X-ray energies. While the X-ray emission may result from the high-frequency tail of the synchrotrons spectrum in X-ray-selected BL Lac objects (Sambruna, Maraschi, & Urry 1996), typical parameters for synchrotrons self-Compton models of radio-selected sources imply that the X-ray emission results from up-scattering of radio or millimeter-wave photons (Marscher & Gear 1985).

We do not have to rely only on light curves of the total flux-density, since we have structural information on the parsec-scale radio jet at several epochs, We can therefore test the predictions of the synchrotrons self-Compton model for each compact component in the jet, and repeat this calculation for each X-ray observing epoch.

4.2. **Constraining Models of the Inverse-Compton Emission**

Our approach in modeling the synchrotrons and SSC emission from 3C 345 is to test the simplest models which are consistent with all the data. We concentrate on the radio and X-ray bands, for which we have the most data, but use non-simultaneous (but close in time) data from other wavebands to constrain the broad-band spectra predicted by the models, Figure 3 illustrates the spectral decomposition of the jet for one of the five X-ray epochs, 1992.67, using the procedure described in Section 1.

From previous VLBI results (e.g. Zensus, Cohen, & Unwin 1995), we know that the core ('D') is inhomogeneous, with a slowly-rising spectrum in the radio. Following Unwin et al. (1994) we modeled the core using the inhomogeneous conical-jet model of Königl (1981), in which the particle density and magnetic field strength fall as power-laws with radius. The rising synchrotrons spectrum in the radio results from superposition of locally-homogeneous emission regions with varying spectral 'turnovers'. In Königl's notation, there is a transition to mostly optically-thin emission at ν_{sM} , and the corresponding 'thick' and 'thin' indices are α_{s1} and α_{s2} respectively. Because we lack simultaneous VLBI imaging above 22 GHz, we have no direct measurement of the core's spectral index on the optically-thin side of the spectrum. We overcome this by making

the reasonable assumption that the source is dominated above ~ 43 GHz by a single (but perhaps inhomogeneous) component. Published 43-GHz images (e.g. Krichbaum et al. 1993) have relatively poor dynamic range, but continue the trend seen at lower frequencies for the jet to be shorter and the core increasingly dominant, with increasing frequency. The spectral index in the mm and sub-mm range is $\alpha_{\text{s}2} \simeq 0.5$ (Gear et al. 1994) as shown in Fig. 3.

There are several additional observational constraints to the Königl model, besides the spectral shape: the angular size of the core at 22 GHz; the observed opening angle ϕ_{obs} of the jet; and the apparent superluminal motion β_{obs} . Of course, superluminal motion is not directly observable within the core, so we took the most reliable measurement closest to the core, $\beta_{\text{obs}} \simeq 3.0$ for C5 (Lobanov 1996).

Table 2 summarizes the principal physical parameters of the nucleus of 3C 345 measured with VLBI, interpolated to the epochs of the X-ray observations, for the period 1992-94. Since the nucleus is obviously inhomogeneous, we treated the spectral indices above and below the spectral turnover as free parameters in the fit. Gaussian component profiles fit the (u , v) about as well as spheres in all cases, but spheres allow simpler comparison with the simplest models of inverse-Compton emission.

Assuming spherical symmetry is clearly a poor approximation to the shape of the individual features, especially the nucleus, though in most cases the data do not require an axial ratio other than unity. The jet width increases with radius (Biretta, Moore, & Cohen 1986), but most of the images have insufficient signal-to-noise ratios to reliably constrain component shapes very close ($\lesssim 1$ mas) to the core. In the case of an inhomogeneous-jet model (e.g. Königl 1981) the angular size of the core (component D) decreases in power-law fashion with frequency. As Unwin et al. (1994) pointed out, this variation can be measured if the core is slightly resolved, even if the shape is poorly constrained. Further out, components are well resolved (Unwin & Wehrle 1992), and clearly require more parameters to describe them; however, these components do not contribute significantly to the X-ray emission,

Results of model fitting for C7 are given in Table 3. Each ‘knot’ in the jet is represented by a homogeneous sphere, and we fit to the (u , v) data for position flux density and angular diameter. We believe that shocks play a role in the evolution of the knots, but the observations do not resolve them enough to justify a more-complicated model. As noted in Section (3), C6 and the other jet components are not significant X-ray producers (except C5 at epoch 1990.55 [Unwin et al. 1994]), because they are weaker and extended. We use them in the model-fitting the VLBI data, but do not consider them further in the context of models of the broad-band spectrum. For the optically-thin side of the spectra, we took $\alpha_{\text{s}} = 0.75$, the value found by Unwin et al. 1994 for knots C5 and C4 (these both had turnover frequencies below 10 GHz). This is also the measured X-ray index, as required in the homogeneous SSC model; the predicted X-ray flux density is a weak function of α_{s} (Cohen 1985). The quoted radii R in Table 3 were obtained by evaluating, at each X-ray epoch, the polynomial expressions for the position of C7 relative to the core from Lobanov (1996). Error estimates in Tables 2 and 3 are approximate, based mainly on a weighted mean of the intrinsic

errors in the model fit data used in each interpolation. We increased the error estimates in cases where the images indicated that components may be blended,

4.3. Model predictions

Because the nucleus is unresolved in X-rays, and we expect a similar power-law spectrum for the SSC models we used to fit the VLBI data, both the nucleus and the jet components could be contributing to the X-ray flux density. Indeed, Unwin et al. (1994) showed that for epoch 1990.55, relativistic motion was required in both the core *and* jet component C5, implying both were X-ray sources. (The relative contributions are uncertain because of likely changes in jet geometry with radius between the nucleus and C5). However, as we show in this Section, the nucleus is *not* the dominant X-ray emitter at later epochs,

For all epochs except the first (1990.55), the Königl (1981) model of the core *under-predicts* the X-ray emission magnitude for a wide variety of model parameters. In fact, the observed parameters over-constrain the model. For instance, (using Königl's notation) fitted values of the parameters (for epoch 1992.67) which determine the spectral shape ($m = 1.9$, $n = 1.7$, and $\alpha_0 = 0.6$) yield $\alpha_{s1} = -0.55$, $\alpha_{s1} = 1.07$, and X-ray spectral index $\alpha_{c2} = 0.86$; these are only in moderate agreement with observation. Then, fitting for the angular size of the jet at 22 GHz, we find two solutions. (a) a 'large-angle' solution ($\theta = 310$), with an intrinsic jet opening angle $2\phi = 21^\circ$, and X-ray flux density which matches the observed value to a factor of ~ 3 ; and (b) a 'small-angle' solution ($\theta = 110$), with $2\phi = 8^\circ$, and X-ray flux density a factor of 20 below the measured value. We regard solution (a) as very implausible because it is inconsistent with the jet geometry deduced from *superluminal* motion of the resolved jet components, as discussed in detail by Zensus, Cohen, & Unwin (1995). We therefore accept the 'small-angle' solution (b). Even $\theta = 110$ is uncomfortably large for the initial jet direction, Requiring a smaller value of θ (which would be more consistent with the kinematics of C7 – see below) requires a reduction in ϕ , which is then inconsistent with the measured size of the nucleus. Observations of other radio jets over a very wide range of scales (e.g. 3C 120 by Walker, Benson, & Unwin 1987, and 3C 273 by Unwin, Davis, & Muxlow 1994) show that bends become less pronounced with distance from the nucleus; this means that extrapolation to smaller radii than can be measured with VLBI is necessarily uncertain. We therefore conclude that an inhomogeneous jet model, which accounts well for the observed radio structure, cannot simultaneously account for the observed X-ray emission.

This conclusion differs from that of Unwin et al. 1994, who applied a Königl model to the first ROSAT observation in 1990.55, and found a consistent set of parameters for the nucleus which predict both the radio and X-ray properties. There are several differences in fitted parameters between the first epoch and the others (Table 2) which interact in a complicated way to give rise to this difference, primarily the relatively flat 'thick' index (they measured $\alpha_{s1} = -0.2$) and small angular size,

By contrast, the homogeneous-sphere model over-predicts the X-ray emission from component C7 by a large factor at each epoch (Table 3), unless there is bulk relativistic motion ($\delta \gg 1$). The implied Doppler factor is a modest function of the input parameters (e.g. Cohen 1985):

$$\delta \propto S_m \nu_m^{-1.32} \xi^{-1.64} S_X^{-0.18}, \quad (1)$$

where we have set $\alpha_s = 0.75$. Since $\delta > 1$ is a secure limit for C7, the most conservative conclusion, in terms of the jet energetic, is that *C7 is the origin of the observed X-rays*, and that the actual Doppler factor must be such as to lower the predicted flux to match the observed flux. The Doppler factor derived by this method is reliable provided that other sources of X-ray emission, whatever their origin, are smaller.

Since jet components are known to move ‘superluminally’ (with $\beta_{\text{obs}} > 1$), we can derive two of the jet kinematic parameters – the angle θ to the line of sight, and the bulk Lorentz factor γ (Unwin & Wehrle 1992). Figure 4 shows the geometric relation between these quantities. β_{obs} was determined by evaluating a polynomial fitted to the component position as a function of time by Lobanov (1996) at each X-ray epoch (and assuming $h = 1$). At each epoch, we measured δ (which is independent of h) for C7 by equating the predicted and observed X-ray flux densities, as in Unwin et al. (1994).

We show in Figure 4 our measurements for C7 at four epochs, from our inverse-Compton X-ray calculations, The point for C5 derived in the same way (Unwin et al. 1994) also shown. We cannot use C5 to measure the path of C7 in this plane, although its position is (just) consistent with the same path. Clearly, fixed values of θ and γ , corresponding to a straight, non-accelerating jet, are inconsistent with the X-ray and VLBI data: C7 must accelerate (γ increasing) as it moves away from the nucleus. In fact, there appear to be two phases in the evolution of C7: (a) a bend away from the line of sight (from $\theta \simeq 2^\circ$ to $\simeq 10^\circ$, and (b) an acceleration from $7 \simeq 5$ to $\gamma > 10$. This trend is also seen in the simple model of the evolution of C7 (Section 5).

A bend of the 3C 345 jet away from the line of sight was derived by Zensus, Cohen, & Unwin (1995), although in a different context. They showed that each of the superluminal components C2 - C5 exhibited increasing β_{obs} with time (or radius R). If the bulk Lorentz factor γ is constant or slowly varying, then a significant increase in θ is required by the data. We see this in the early stages of the evolution of C7 in our data. However, there are important differences, most notably the range of radius through which each component is followed: Zensus, Cohen, & Unwin followed C2 - C5 from $R \sim 0.4$ to ~ 5 mas, while we measure C7 from $R \sim 0.1$ to ~ 0.5 mas. We deduce $\theta \simeq 10^\circ$ at $R = 0.5$ mas for C7, whereas at a similar radius in the mid- 1980s, C4 and C5 were probably much closer to the line of sight (Zensus, Cohen, & Unwin 1995).

The differences in inferred kinematics between C4, C5, and C7 probably reflect real changes in jet properties, with a characteristic timescale of about two years. Lobanov (1996) points out that the trajectories, projected onto the sky, of all three components are strikingly different, so it should not be surprising that our estimates of θ should show large variations,

5. Discussion

We have shown that the X-ray flux density of 3C 345 is correlated with the high frequency radio flux density, during 1991 - 1993. Of course, the X-ray data are very under-sampled, so we have to retain the possibility that the source is variable on timescales less than a few months, and the correlation is fortuitous. Unfortunately, this timescale had not been sampled adequately for any other blazar until the launch of the Rossi X-ray Timing Explorer (RXTE) in December 1995. However, our simple SSC model predicts just such a strong correlation.

Relativistic beaming plays a key role in making 3C 345 a bright object. In fact, variations in Doppler boosting may well overwhelm any changes in intrinsic (i.e. comoving) luminosity. For C7, the inferred Doppler factor decreased by a factor of three during our monitoring period (Figure 4). Since Doppler boosting is $\propto \delta^{3+\alpha}$, the measured change in δ (Table 3) implies that the intrinsic X-ray luminosity of C7 decreased by a factor of between 5 and 50 (allowing for uncertainties in δ), with the strongest X-ray flux density occurring less than a year after the emergence of C7 from the nucleus (Lobanov 1996). In a homogeneous IC model, Doppler boosting will affect both radio and X-rays, but not equally (cf. Eqn.1), because quantities are referenced to the observer's frame, not the frame co-moving with C7. This has important observational implications, because VLBI images have a limited dynamic range, and X-ray detectors have limited sensitivity: our ability to identify and follow X-ray emitting superluminal features is dependent on changes in intrinsic luminosity and Doppler boosting working together to limit the range of observable flux density variations.

A complete understanding of the broad-band emission process in the nuclei of blazars must include the broad-band spectrum, variability (and its dependence on frequency), and spatial structure on scales below a few pc. The scope of these studies is still limited by observation. A number of models have been devised (see review by Marscher 1996) which may be distinguished by time lags between variability in different bands. Such data are hard to obtain over the timescales of interest, which in 3C 345 range from a month to at least a year,

3C 345 offers a well-sampled picture of the parsec-scale evolution, via the long-term VLBI imaging program (Wardle et al. 1994; Zensus, Cohen, & Unwin 1995; Zensus et al. 1996), Qian et al. (1996) have developed models based on the hypothesis that the component trajectories are confined to the surface of a narrow cone which traces the mean jet direction. In their model, the Doppler factor for component C4 (visible 1980- 1988) decreases from $\delta \simeq 10.8$ to $\simeq 7.0$ over a period of about 3 years. We see a similar decrease in the Doppler factor of C7 (Fig. 4).

The most extensive recent multiwavelength (including optical) campaign on 3C 345 was by Webb et al. (1994), from 1990 November to 1991 May. Unfortunately, these data lie in a large gap in our X-ray coverage, and hence are not directly applicable. Nevertheless, their conclusion that the outburst extended at least from radio through UV, with differing rise times, is consistent with the SSC model we used above to derive the jet kinematics: the flare phenomenon is intrinsically very broad-band. More recently, Stevens et al. (1996) have presented results of flux-density monitoring from radio through sub-millimeter wavelengths, covering about the same time range as our X-ray

data: 1991- 1994. They showed that the evolution of the flare seen in all wavebands (see Figure 1), after subtracting a ‘quiescent’ synchrotrons spectrum, can be modeled as a shock which evolves as it moves down the jet. This shock, which is seen in the phase where expansion losses dominate (Marscher & Gear 1985), is consistent with two cases: either (i) a straight, non-accelerating, non-adiabatic jet, or (ii) an adiabatic jet which curves away from the line of sight.

We can also compare case (ii) of Stevens et al. with our result for the kinematics of component C7. They parametrize the jet curvature as a change in the Doppler factor δ (possibly of a new component C8) as a power-law, with $\delta \propto R^{-c}$, where $c = 0.22$. If we assume a similar relation and fit for the exponent, we obtain $c = 0.81$, through the fit is fairly poor. These values of c both indicate a decrease in the Doppler factor of C7 during roughly the same time period. Since they were derived completely independently using (mostly) different data, we do not regard the different values as conflicting, Since β_{obs} is also a function of R , we can compute the relation between δ and β_{obs} that the power-law expression implies. This is shown as the heavy curve in Figure 4; note that time (and radius) increases along this curve with decreasing δ .

These two measurements of a secular change in δ contrast with modeling by Lobanov & Zensus (1996) who found that the evolution of components C4 and C5 during the mid-1980s is consistent with a shock-in-jet model (Marscher & Gear 1985), but only if the Doppler factor is an increasing function of radius. They require c in the range -0.6 to -1.0 to make the rest-frame turnover frequency remain almost constant or decrease with time, as required as the shock emission develops (Marscher 1990). There are several possible reasons for this apparent discrepancy. (a) C4 and C5 may evolve differently from component C7 which we have studied here. (b) Their measurements were mostly made at more than 1 mas from the nucleus; our C7 data are all within $R = 0.5$ mas, where the physical conditions may be quite different, or we are studying the same shock process, but at a much earlier stage. (c) We used measured angular sizes for C7 at each epoch, rather than assuming size $\propto R$ (i.e. a conical geometry).

Finally, we consider the lack of detectable γ -rays from 3C 345. The 2- σ upper limit from the EGRET instrument on CGRO (Fichtel et al, 1994) corresponds to $\simeq 3 \times 10^{-10}$ Jy at 100 MeV, assuming a photon index $\Gamma = 2.0$, as measured by Fichtel et al. for 3C 279. Between the X-ray and 7-ray ranges, the mean spectral index must be $\alpha > 0.68$. The SSC models discussed in Section 4.3 should be applicable in the EGRET band, provided the synchrotrons cutoff lies in the UV range or above. Using parameters derived for the inhomogeneous jet (Königl) model of the nucleus, we find a predicted γ -ray flux at least a factor 100 below the EGRET upper limit in the ‘small-angle’ case, but only a factor of two below for the ‘large-angle’ solution. While we prefer the small-angle solution for consistency with both the parsec-scale kinematics and the X-ray and γ -ray data, a γ -ray detection at only slightly below the EGRET upper limit would cast doubt on this interpretation, but could be accommodated by adjusting other parameters in the model.

For component C7, we extrapolated the SSC spectrum from X-rays to γ -rays, using the (sphere) model parameters in Table 3, again assuming the synchrotron spectrum extends into the UV range. Using the Doppler factor derived from the X-rays at each epoch, we find the sphere model under-

predicts the γ -ray flux by a factor of 2-3. This prediction is fortuitously close to the EGRET upper limit; it is quite sensitive to the assumed spectral index, and to the Doppler factor. Reducing δ at each epoch by only 15-20 % would raise the predictions to the EGRET limit. Thus the lack of detectable γ -rays from 3C 345 is consistent with an extrapolation of the SSC models. However, a future detection at a level well below the present limit would invalidate many of the derived source parameters,

Finally, we compare 3C 345 with one of the best studied blazars, 3C 279 ($z = 0.538$), with which it shares many properties, except that 3C 279 is a strong γ -ray source. Results from multiwavelength campaigns have been presented by Maraschi et al. (1994) and Hartman et al. (1996). A striking difference is that 3C 279 is a strong γ -ray source (von Montigny et al. 1995). It is the only blazar for which well-sampled simultaneous X-ray and γ -ray data are available; in February 1996, an outburst was seen lasting about 2 days, highly correlated in the two bands (McHardy 1996). This result provides a clue as to why 3C 345 is a strong X-ray source but is not detected in γ -rays. In 3C 279 the γ -rays, and the variable part of the X-ray emission, must come from a very small volume (a few light-days times δ), presumably very close to the central black hole. But we have shown that the detected X-ray emission from 3C 345 came from a jet component $\simeq 1$ pc in size, at a distance of $\simeq 2$ pc from the nucleus, during the period 1991 - 1993, with a variability timescale of several months, rather than days. Therefore, at that time, the lack of detectable γ -rays from 3C 345 is related to the fact that *nucleus* was not emitting X-rays. This could be due either to an 'unfavorable' geometry at the base of the jet (radius $\ll 1$ pc), or intrinsically weak emission on the smallest length scales. In support of the latter explanation, we note that 3C 345 is unusual among blazars in having a discernible 'blue bump' in the optical/UV (Webb et al. 1994), implying that the power-law contribution" from the most compact part of the jet makes a smaller contribution to the overall spectrum than in say, 3C 279. On this basis, we might expect γ -rays to be detectable in the future, if the jet kinematics change so as to beam high-energy emission into our line of sight.

6. Summary

We have presented a series of X-ray flux density measurements of the superluminal quasar 3C 345 over a period of three years, made with the 0.2 -2.0 keV PSPC instrument on ROSAT. Using multiwavelength VLBI imaging of the parsec scale jet, we have deduced the spectral shapes and angular sizes of the main jet components at each of the X-ray epochs, and developed a kinematic model which is consistent with all the available data. In particular, we have studied time *variability* in the predicted X-ray flux density from a simple homogeneous synchrotrons self-Compton model of one of the superluminal jet components,

Testing of the various models of broad-band energy emission process in AGN is very dependent on observational campaigns which monitor variability across many wavebands. A definitive observation of this kind has yet to be made, though recent campaigns on 3C 345 (Webb et al. 1994) and 3C 279 (Maraschi et al. 1994, Hartman et al. 1996) are beginning to address the key model

discriminants (see review by Marscher 1990).

The present work on 3C 345 uses the best data available on any object studied with VLBI; even so, there are limitations, as discussed above, High-frequency VLBI imaging is the most important improvement - fortunately, it is now possible to routinely make high dynamic-range images at 43 GHz with the VLBA; with monitoring at this frequency we can probe the smallest jet scales, where we believe the X-ray emission is strongest, and derive sizes and optically-thin spectral indices for individual components. In addition, rapid frequency-switching on the VLBA makes simultaneous multifrequency imaging relatively straightforward. VLBA imaging, coordinated with monitoring by recently-launched RXTE satellite should allow future multifrequency programs -of many AGN, not just one or two selected objects - to build a complete picture of the broadband variability of AGN.

The main results of the present work may be summarized as follows:

1. The soft X-ray flux density of 3C 345 measured by ROSAT correlates directly with the high-frequency radio flux density: a broad outburst is seen during 1992-1993 in both bands. Correlated variability is expected in models which involve generation of X-rays by the synchrotrons self-Compton (SSC) process in the most compact jet components. In 3C 345, previous work showed that the nucleus and the jet components closest to the core are the dominant X-ray emitters (Zensus, Cohen, & Unwin 1995).
2. The core of 3C 345 (component 'D') can be modeled with an inhomogeneous jet, which explains the radio properties, most notably the inverted (but almost flat) radio spectrum. However, the model under-predicts the observed X-ray flux, so its contribution, at least in 1991-1993, was probably negligible.
3. Jet component C7 (the brightest and most compact in 1992- 1993), and *not the* nucleus, is the origin of the X-ray emission, unless the Doppler factor δ of the jet is even larger than the limits we derive. If C7 is indeed the sole source of X-rays, then the Doppler factor of C7 decreased from $\delta \approx 12$ to ≈ 4 during 1992-1993, Stevens et al. (1996), using more extensive multifrequency data than available to us (but no X-ray data), also found that the jet Doppler factor decreased during this time period.
4. The SSC models for the nucleus and jet component C7 are consistent with CGRO/EGRET upper limit on the γ -ray flux from 3C 345, although a detection at well below the present limit would modify our derived model parameters substantially.
5. Kinematic data for component C7 from Lobanov & Zensus (1996) show that its apparent superluminal speed β_{obs} increases with time. For consistency with our measurement of the Doppler factor, the path of C7 in three dimensions must begin close to the line of sight (epoch 1992.0), at $\theta \approx 2^\circ$, then bend away to $\theta \approx 10^\circ$ as it passes a point ≈ 0.4 mas from the nucleus (epoch 1993.1). During this time period, the Lorentz factor of C7 remains constant at $\gamma \approx 5$.

6. After 1993.1, C7 must accelerate to $\gamma \gtrsim 10$ to be consistent with the measured increasing superluminal speed and decreasing Doppler factor.

This research has made use of data from the University of Michigan Radio Astronomy Observatory which is supported by the National Science Foundation (grant AST-9421979) and by funds from the University of Michigan. We are grateful to Harri Teräsraanta (Helsinki University of Technology) for providing radio flux-density monitoring data in advance of publication. S. Snowden and M. Corcoran helped with the analysis of PSPC data, We thank J. Stevens for data in advance of publication, and A. Marscher for valuable discussions, The National Radio Astronomy Observatory is a facility of the National Science Foundation, operated under cooperative agreement by Associated Universities, Inc. This work was supported in part by NSF grant AST 9117100, NASA grants NAG 5-2167 and 7-1260, and the NASA Long Term Space Astrophysics program.

A. Determining PSPC fluxes in detector regions obscured by window support ribs

The entrance window of the ROSAT Position-Sensitive Proportional Counter (PSPC) is supported by a fine mesh and a coarse rib structure, In some cases, an image of a source of interest may land on the support rib, However, the region of the PSPC covered by the ribs is sufficiently far off-axis such that the size of the image of a point source -- which is then larger because of the degraded point-spread function -- is comparable or bigger than the width of the ribs, so some of the source photons are always detected. To further minimize the effect of the mesh and the ribs on the resulting data, the satellite is normally operated in a 'wobble' mode, such that the spacecraft attitude oscillates along one axis with a fixed period (typically 400 seconds). This causes source obscuration for most positions on the detector to occur at most only a part of the time, and in many cases, makes it possible to measure reasonably accurately fluxes of partially obscured point sources. The procedure below describes how an off-axis, rib-obscured data can be corrected for the rib obscuration and specifically *not* for the vignetting, as the latter is done automatically under the standard procedures for the PSPC data reduction using FTOOLS (Blackburn 1996).

The procedure to recover the flux of a source partially obscured by the ribs involves a generation of an 'exposure map', and then correcting the original image by dividing it by such an exposure map, normalized to the nominal exposure. Such a map needs to be generated separately for every observation, as the combination of the spacecraft attitude and the wobble is unique. First, if the image corresponding to the relevant observation is not available, it can be produced from the archived events file using the FTOOL XSELECT, and scaled to 512 x 512 pixels. The generation of the exposure map is normally accomplished using the FTOOL PCEXPMAP operating on this image, making sure that the vignetting correction is *not* applied. The resulting exposure map is then normalized such that the on-axis fractional exposure is unity. This is accomplished by dividing the exposure map generated as above by the 'true' (on-axis) exposure, using the FTOOL FCARITH.

The next step is to divide the original image by this fractional effective exposure map, using the FTOOL **FARITH**. This generates an essentially obscuration-corrected (but, again, not vignetting-corrected) image of the field. (Note that using the FTOOL **PCARF** will include the vignetting correction in generation of the off-axis response.) Finally, the obscuration correction (which should be a number larger than unity but less than \sim a few) can be determined by taking the ratio of a sum of pixel values collected in the same source extraction region of two images, the exposure-corrected and the original; this can be accomplished using the FTOOL **IMCNTS** on both images. Further data reduction is carried out in a standard manner, where the off-axis effects on the telescope effective area (both energy dependence and vignetting) are included in the Ancillary Response File, generated via the FTOOL **PCARF**, and the obscuration correction to the flux is then applied manually. Using this procedure, one can use the standard PSPC Redistribution Matrix File appropriate to the PSPC 'B' or 'C' detector, as appropriate for the particular observation.

REFERENCES

- Aller, M. F., Aller, H. D., & Hughes, P. A. 1992, ApJ, 399, 16
- Biretta, J. A., Moore, R.L., & Cohen, M. H. 1986, ApJ, 308,93
- Blackburn, J. K. 1996, Users Guide to FTOOLS Release 3.5 (NASA: Goddard Space Flight Center)
- Bloom, S.D. & Marscher, A. P. 1996, ApJ, 461,657
- Bregman, J. N. et al. 1986, ApJ, 301, 708
- Brown, L. F., Roberts, D. H., & Wardle, J. F. C. 1994, ApJ, 437, 108
- Cawthorne, T. V., Wardle, J. F. C., Roberts, D. H., & Gabuzda, D. C. 1993, ApJ, 416,519
- Cohen, M. H. 1985, in Extragalactic Energetic Sources, ed. V. K. Kapahi (Indian Academy of Sciences, Bangalore),1
- Cohen, M. H. et al. 1983, ApJ, 272,383
- Elvis, M., Lockman, F. J., & Wilkes, B. J. 1989, AJ, 97, 777
- Fichtel, C. et al. 1994, ApJS, 94,551
- Gear, W. K. et al. 1994, MNRAS, 267, 167
- Guijosa, A. & Daly, R. A. 1996, ApJ, 461,600
- Hagen-Thorn, V. A., Marchenko, S. G., Takalo, L. O., & Sillanpää, A. 1996, A&A, 306,23
- Hartman, R. C. et al. 1996, ApJ, 461,698

- Hewitt, A. & Burbidge, G. 1993, ApJS, 87,451
- Impey, C. D. & Neugebauer, G. 1988, ApJ, 95,307
- Kollgaard, R. I., Wardle, J. F. C., & Roberts, D. H. 1989, AJ, 97', 1550
- Königl, A. 1981, ApJ, 243, 700
- Krichbaum, T. P. et al. 1993, A&A, 275,375
- Leppanen, K. J., Zensus, J. A., & Diamond, P. J. 1995, AJ, 110,2479
- Lobanov, A. P. 1996. PhD thesis, New Mexico Institute of Mining and Technology
- Lobanov, A. P. & Zensus, J. A. 1996, ApJ. in press
- Maraschi, L. et al. 1994, ApJ, 435, L91
- Marscher, A. P. 1990, in Parsec-Scale Radio Jets, ed. J. A. Zensus and T. J. Pearson (Cambridge: Cambridge University Press), 280
- Marscher, A. P. 1996, Proc. Nat. Acad. Sci., 92, 11439
- Marscher, A. P. & Gear, W. K. 1985, ApJ, 298, 114
- McHardy, L 1996, in Workshop on Blazar Variability, Florida International University, in press
- Moore, R. L. & Stockman, H. S. 1984, ApJ, 279,465
- Morrison, R. & McCammon, D. 1983, ApJ, 270, 119
- Murphy, D. W., Browne, I. W. A., & Perley, R. A. 1993, MNRAS, 264,298
- Qian, S. J., Krichbaum, T. P., Zensus, J. A., Steffen, W., & Witzel, A. 1996, A&A, 308,395
- Readhead, A. C. S. 1994, ApJ, 426,51
- Sambruna, R. M., Maraschi, L., & Urry, C. M. 1996, ApJ, 463,444
- Shafer, R. A., Haberl, F., Arnaud, K. A., & Tennant, A. F. 1990, XSPEC Users' Guide, Version 2 (Noordwijk: ESA TM-09)
- Steffen, W., Zensus, J. A., Krichbaum, T. P., Witzel, A., & Qian, S. J. 1996, A&A, 302,335
- Stevens, J. A., Litchfield, S. J., Robson, E. I., Cawthorne, T. V., Aller, M. F., Aller, H. D., Hughes, P. A., & Wright, M. H. C. 1996, ApJ, 466, 158
- Unwin, S. C., Davis, R. J., & Muxlow, T. W. B. 1994, in Compact Extragalactic Radio Sources, ed. J. A. Zensus & K. I. Kellermann, (Green Bank: National Radio Astronomy Observatory), 81

- Unwin, S. C. & Wehrle, A. E. 1992, ApJ, 398, 74
- Unwin, S. C., Wehrle, A. E., Urry, C. M., Gilmore, D. M., Barton, E. J., Kjerulf, B. C., Zensus, J. A., & Rabaça, C. R. 1994, ApJ, 432, 103
- von Montigny, C. et al. 1995, ApJ, 440, 525
- Walker, R. C., Benson, J. M., & Unwin, S. C. 1987, ApJ, 316, 546
- Wardle, J. F. C., Cawthorne, T. V., Roberts, D. H., & Brown, L. F. 1994, ApJ, 437, 122-135
- Webb, J. R. et al. 1994, ApJ, 422, 570
- Zensus, J. A., Cohen, M. H., & Unwin, S. C. 1995, ApJ, 398, 74
- Zensus, J. A., Lobanov, A. P., Leppanen, K. J., Unwin, S. C., & Wehrle, A. E. 1996, in preparation

Fig. 1.— X-ray, radio and millimeter-wave flux monitoring of 3C 345, during 1990- 1993, The X-ray flux densities from Table 1 have been scaled by a factor 10^6 before plotting. Radio through millimeter data are from Stevens et al. (1996), who show the complete flare history in the range 5 -375 GHz. Error bars for the 37 and 90 GHz curves are omitted for clarity; a solid line connects the 14.5-GHz points, also for clarity. Monitoring data at 5 and 8 GHz (not shown here) exhibit the characteristic behavior seen in many blazar flares, namely a delayed, broader peak relative to the higher frequencies, with a slow decline thereafter. Hence the decline in X-ray flux after $\simeq 1992.0$ is strongly correlated with the radio data only above 37 GHz.

Fig. 2.— VLBI image of 3C 345 at 22 GHz, at a resolution of 0.7 pc, at epoch 1992.86. Contours at -0.25, 0.25, 0.5, 1, 2, 4, 8, 16, 32, and 64 % of the peak (4.12 Jy/beam). Beam FWHM = 0.44 x 0.18 mas, in P.A. 0.6° . This image is representative of a long series of monitoring experiments at 5, 8, 11, and 22 GHz, Labeled features are the nucleus 'I', and superluminal jet components C4, C5, C6 and C7, which are identified at other epochs and frequencies, allowing us to follow their spatial and spectral evolution.

Fig. 3.— Radio spectrum of 3C 345 and parsec-scale superluminal components in its jet, at epoch 1992.67. Total flux density measurements are from the UMRAO database (4.8, 8.0, and 14.5 GHz), and Gear et al. 1994, Stevens et al, 1996 (37 -375 GHz); a dashed curve joins those measurements, which are all within about one month of the X-ray epoch; variability on that timescale, while easily measurable, dots not alter the spectral shape much. Flux densities for the nucleus (D) and the dominant jet components at this epoch (C6, C7) are derived from VLBI imaging, as described in the text, A dotted line shows the fit of a homogeneous sphere model to C7 (assuming $\alpha = 0.75$ above the turnover). The solid curve represents the fit of a Königlinhomogeneous jet model to the nucleus, with the spectral slopes above and below the break treated as free parameters; note that the inhomogeneous jet is assumed to dominate the total flux above ~ 50 GHz.

Fig. 4.— Geometry and kinematics of the jet in 3C 345. The Doppler factor δ (from X-rays) and superluminal speed β_{obs} are *observable* quantities; the angle θ to the line of sight, and the bulk Lorentz factor γ are *derived* quantities, Measurements of component C7, whose superluminal speed increases monotonically with time (or radius R), are shown as filled circles. The open circle represents C5, which dominated the jet in 1990 (Unwin et al. 1994). The heavy curve shows the evolution of C7 (towards smaller δ) assuming the relation $\delta \propto R^{-0.81}$ (see Section 5),

Table 1. ROSAT PSPC Observations of 3C 345

Observation number	Observation date (DDMMYY)	Exposure (s)	Count rate (s ⁻¹)	Count rate error (s ⁻¹)	Vignetting ratio	Rib covering ratio	Flux density at 1 keV (μJy)
015	19/07/90	4086	0.29	0.01	1.00	1.00	0.41
428	16/01/92	3899	0.28	0.01	0.82	0.53	0.93
869	01/09/92	4219	0.50	0.01	1.00	1.00	0.77
843	03/09/92	2857	0.29	0.01	0.78	0.71	0.81
870a	06/03/93	2985	0.28	0.01	1.00	1.00	0.45
870b	11/03/93	3001	0.30	0.01	1.00	1.00	0.48
428a	19/07/93	946	0.18	0.02	0.85	0.51	0.49

Note. — Count rate is net (background-subtracted) counts/s, uncorrected for vignetting. Vignetting is the ratio of effective area to that of the telescope alone. Rib covering ratio is the effective area including PSPC rib obscuration divided by the unobscured area, 1 keV flux density is in microJansky, corrected for a Galactic absorbing column of $N_{\text{H}} = 0.74 \times 10^{20} \text{ cm}^{-2}$, and adopting a mean spectral index $\alpha = 0.74$. The estimated systematic error on the 1-keV flux for the on-axis observations (with vignetting ratio = 1.0) is $\sim 5\%$, while for the off-axis observations it is $\sim 10\%$.

Table 2. Radio Parameters of the Nucleus of 3C 345

E p o c h ^a	S_m (Jy)	ΔS_m^b (Jy)	ν_m (GHz)	$\Delta \nu_m$ (GHz)	α_{s1}^c	α_{s2}	ξ_{22}^d (mas)	$\Delta \xi_{22}$ (mas)	ξ_8 (mas)	$\Delta \xi_8$ (mas)
1990.55	2.5	-	200	-	-0.20	0.75	0.18	-	0.60	-
1992.05	12	1	35	5	-1.18	0.95	0.26	0.03	-	-
1992.67	9	1	55	5	-0.76	0.95	0.28	0.03	0.39	0.08
1993.19	7	1	50	5	-0.51	0.95	0.32	0.02	0.16	0.1
1993.55	6.5	1	50	5	-0.49	0.95	0.37	0.02	0.15	0.1

^aData interpolated to epochs of ROSAT PSPC observations

^bErrors are nominally 1- σ , but are dominated by systematic errors which are included in the estimate

^c α_{s1} and α_{s2} are the (partially) optically thick and thin spectral indices (Königl 1981)

^dAngular size of a sphere fitted to the VLBI (u, v) data (22 and 8 GHz), and interpolated to the X-ray epoch. Angular resolution at 5 GHz is insufficient for reliable measurement of the nucleus

Table 3. Radio Parameters of Jet Components C5 and C7 of 3C 345

Epoch ^a	Component	R^b (mas)	S_m^c (Jy)	ΔS_m (Jy)	ν_m (GHz)	$\Delta \nu_m$ (GHz)	α_s^d	ξ^e (mas)	$\Delta \xi$ (mas)	δ_{\min}^f	$\Delta \delta_{\min}$
1990.55	C5	1.75	3.2	0.5	2.7	0.5	0.75	0.80	-	8.0	3.5
1992.05	C7	0.14	4.6	0.5	12.8	0.5	0.75	0.20	0.04	11.7	4.1
1992.67	C7	0.22	7.0	0.5	12.5	1.0	0.75	0.35	0.02	6.5	0.9
1993.19	C7	0.38	5.1	0.5	11.6	0.5	0.75	0.41	0.02	5.5	0.6
1993.55	C7	0.52	3.1	1.0	11.0	1.5	0.75	0.38	0.02	4.0	1.1

^aData interpolated to epochs of ROSAT PSPC observations

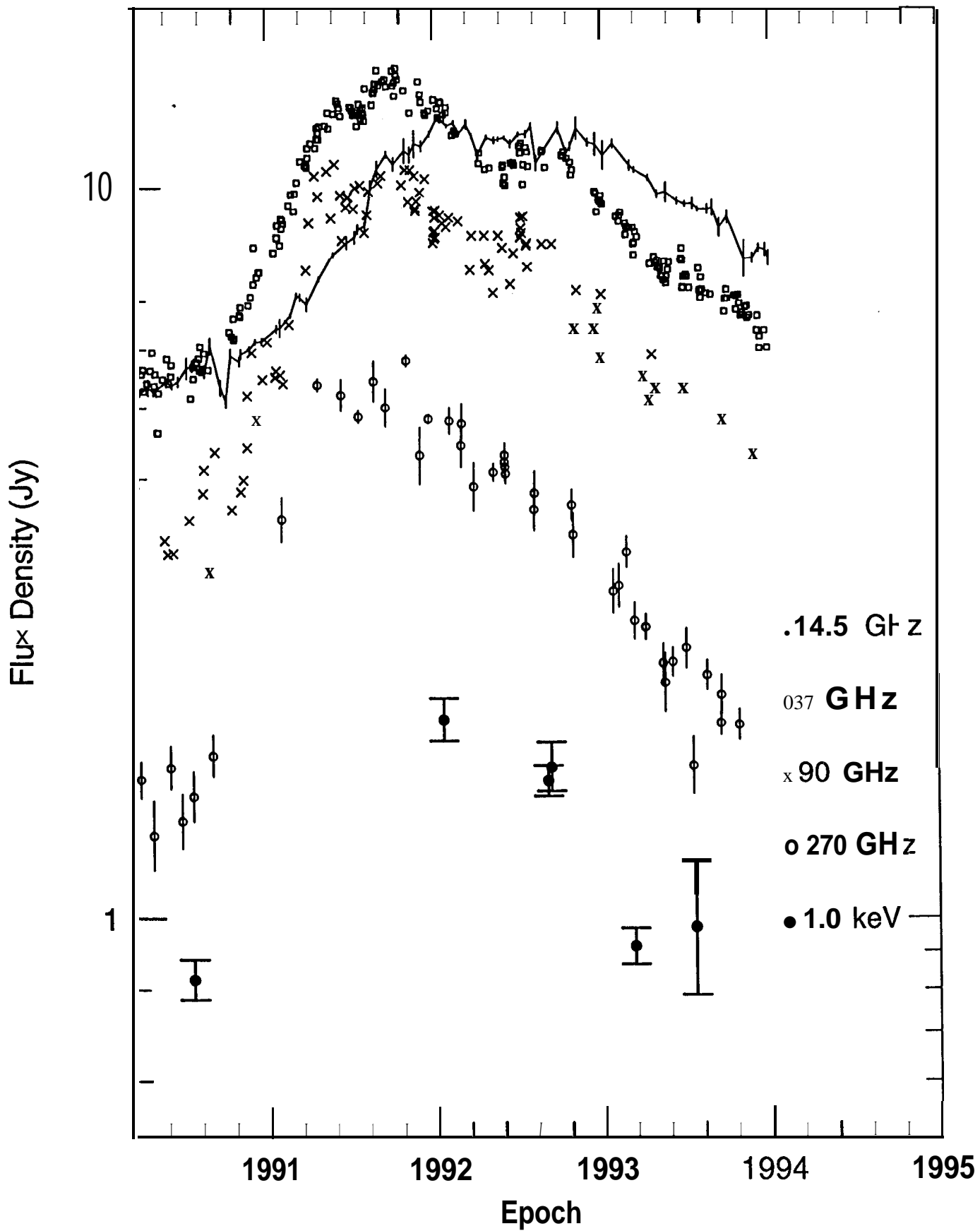
^bDistance from the nucleus, evaluated from polynomial $R(t) = \sum a_n t^n$ (Lobanov 1996)

^cSpectral turnover parameters from fitting a homogeneous sphere model to component spectrum (cf. Fig. 3). Errors are nominally 1- σ , but are dominated by systematic errors which are included in the estimate

^dOptically-thin spectral index α_s assumed in deriving the spectral turnover

^eAngular size of a sphere fitted to the VLBI (u, v) data, and interpolated to the X-ray epoch

^fMinimum allowed Doppler factor, taking the observed X-ray flux density as an upper limit to the IC emission from C7. Errors include quadrature contributions from the input parameters



3C345 SVLNGKPLNBOH 22.229 GHz 1 1/1 1/92

